# Third-order elastic constants and acoustic-mode vibrational anharmonicity of antimony

G. A. Saunders
*School of Physics, University of Bath, Claverton Down, Bath BA2 7AY, United Kingdom*

Y. K. Yoğurtçu
*Atatürk Universitesi, Fen-Edebiyat Fakültesi, Fizik Bölümü, Erzurum, Turkey*
(Received 13 March 1984)

Measurements of the effects of hydrostatic and uniaxial pressures on ultrasonic wave velocities are used to obtain the 14 third-order elastic constants and also the hydrostatic pressure derivatives of the second-order elastic constants of antimony. The experimental data are used to calculate the zone-center acoustic-mode Grüneisen parameters in the long-wavelength limit on the basis of generalized Grüneisen theory in the quasiharmonic approximation. The results suggest that the negative value at low temperatures of the linear thermal expansion coefficient tensor component $\alpha_{11}$ arises from the dominant contribution of long-wavelength shear modes having negative mode Grüneisen parameters. In general elastic behavior, the vibrational anharmonicity and the thermal expansion are consistent with the tendency of antimony to exhibit a layerlike character.

## I. INTRODUCTION

The effects of hydrostatic and uniaxial pressure upon ultrasonic wave velocities have been measured in the rhombohedral $A7$ structure (point group $\bar{3}m$) semimetal antimony. The results have been used to obtain sets of the 14 third-order elastic constants (TOEC) and the hydrostatic pressure derivatives of the 6 second-order elastic constants (SOEC) for this element. The first information of the effect of hydrostatic pressure on the lattice dynamics of the group-V semimetals bismuth, antimony, and arsenic was obtained by Richter *et al.*,[1] who found that ultrasonic wave velocities increased while the zone-center optical-mode frequencies decreased with applied pressure. A complete set of the TOEC of bismuth[2] and the hydrostatic pressure derivatives of the elastic constants of bismuth-antimony alloys[3] are also available. The TOEC are of particular interest because they are related to the anharmonic properties of crystals as the coefficients of the first-order anharmonic terms in the interatomic potential. Thus they provide quantitative information of the nonlinear behavior of the crystal under a finite strain and hence of the vibrational anharmonicity of the acoustic phonons at the long-wavelength limit. An interesting characteristic of the group-V semimetals is that they show a progressive tendency to behave as layerlike crystals. Although to describe antimony (or even arsenic) as having a layer structure is an oversimplification, its TOEC give an indication of the nonlinear acoustic behavior which can be expected of this type of crystal. To interrelate the influence of acoustic-mode vibrational anharmonicity with thermal expansion, the TOEC data have been used to calculate the mode Grüneisen parameters at the long-wavelength limit in the anisotropic continuum model. These parameters clearly identify the particular acoustic shear modes which are responsible for the negative thermal expansion coefficient ($\alpha_{11}$) below 20 K in antimony.[4]

## II. EXPERIMENTAL PROCEDURE AND RESULTS

The single-crystal boule of antimony, grown by zone refining of 99.999%-purity starting material, was aligned to within $\pm 1/2°$ by using Laue x-ray back-reflection photography. To determine the signs of certain elastic constants for a material belonging to the $\bar{3}m$ point group, it is necessary to orientate the crystal unambiguously with respect to the atomic arrangement in the crystal; this was achieved using a standard Laue back-reflection procedure.[5,6] Monocrystalline rectangular parallelepipeds (dimensions approximately $1\times1\times1$ cm$^3$), suitable for the propagation of ultrasonic waves and the application of uniaxial pressure in the crystallographic directions specified in Table I of Ref. 2, were then cut by spark erosion. Sample faces were then spark planed to a parallelicity of approximately $10^{-4}$ rad. To obtain a set of TOEC, the hydrostatic and uniaxial pressure dependences of ultrasonic wave velocities were measured using apparatus and techniques described elsewhere.[7] To bypass calculation of the changes in crystal dimensions induced by hydrostatic pressure, the experimental data were transformed to correspond to the "natural velocity" $W$.[8] Experimental results obtained for the dependence of the natural velocity of ultrasonic waves upon hydrostatic and uniaxial pressure are given in Figs. 1 and 2.

Equations relating the second-order elastic stiffness tensor components $C_{IJ}$ with the ultrasonic wave velocity have been developed for rhombohedral $RI$ ($\bar{3}m$ Laue group) crystals from the Christoffel equations by several authors.[9–11] The adiabatic second-order elastic stiffness components of antimony have been computed, using a least-mean-squares fit procedure of the measured ultrasonic wave velocities to these equations. The previous data for the elastic constants are rather widespread; the comparison, given in Table I, shows that the present results are close to those of Epstein and de Bretteville[12] which were also measured by a pulse-echo ultrasonic tech-

 

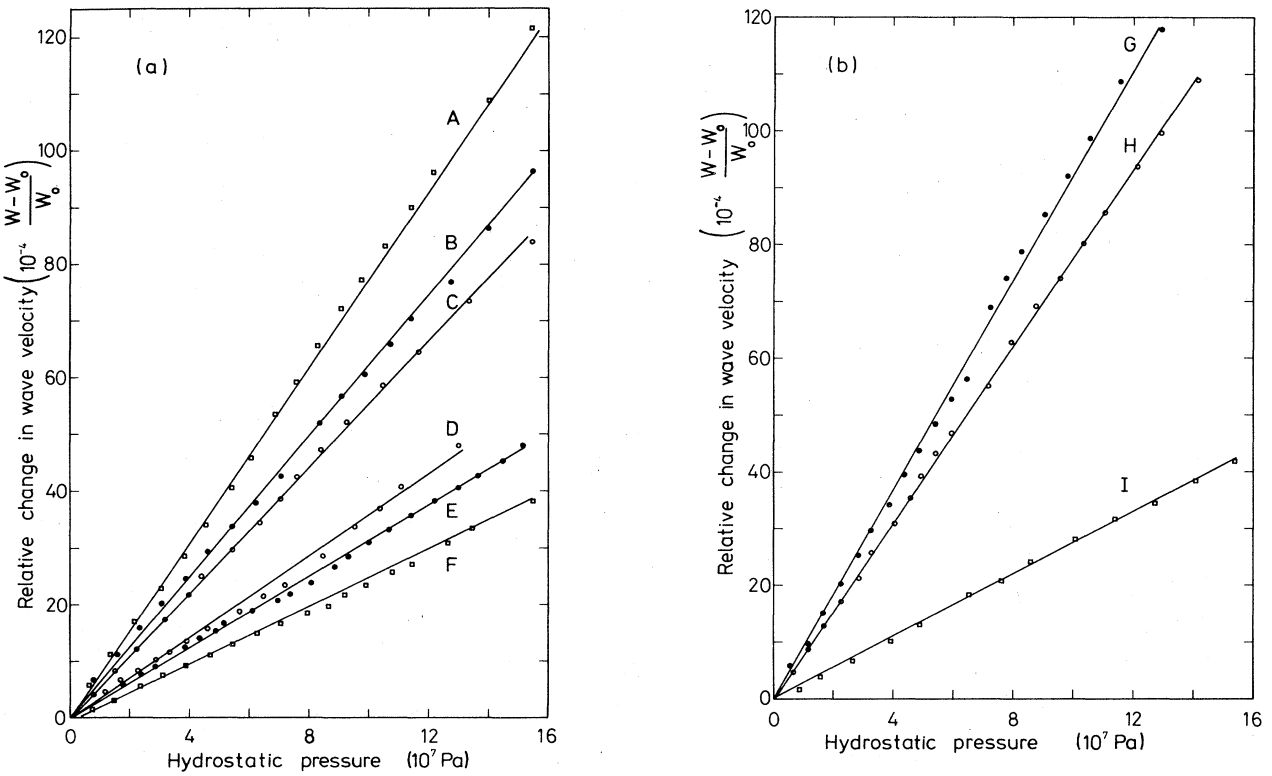


FIG. 1. Relative change induced in the natural wave velocity in antimony through the application of a hydrostatic pressure. The modes are (a) *A*, $\vec{N}||[0\,1/\sqrt{2}\,1/\sqrt{2}]$, $\vec{U}||[0\,1/\sqrt{2}\,1/\sqrt{2}]$; *B*, $\vec{N}||[0\,-1/\sqrt{2}\,1/\sqrt{2}]$, $\vec{U}||[0\,-1/\sqrt{2}\,1/\sqrt{2}]$; *C*, $\vec{N}||[0\,1/\sqrt{2}\,1/\sqrt{2}]$, $\vec{U}||[0\,-1/\sqrt{2}\,1/\sqrt{2}]$; *D*, $\vec{N}||[010]$, $\vec{U}[100]$; *E*, $\vec{N}||[100]$, $\vec{U}||[100]$; *F*, $\vec{N}||[0\,1/\sqrt{2}\,1/\sqrt{2}]$, $U||[100]$, (b) *G*, $N||[001]$, $\vec{U}||[001]$; *H*, $\vec{N}[001]$, $\vec{U}$ in (001) plane; *I*, $\vec{N}||[0\,-1/\sqrt{2}\,1/\sqrt{2}]$, $\vec{U}||[100]$.

nique. The early results of Bridgman[13] were obtained using a static pressure method and so correspond to isothermal stiffnesses; however, the isothermal-to-adiabatic correction is negligible. The results of Leventhal[14] were obtained by a pulse technique but lie well outside the error range in either the present work or that of Epstein and de Bretteville;[12] that is particularly true of $C_{11}$ and $C_{33}$, which are the easiest elastic stiffnesses to obtain with the highest accuracy. The elastic compliances (Table I) also show close agreement with the results obtained by Epstein and de Bretteville.[12]

Knowledge of the directions in a crystal along which pure elastic modes can propagate is particularly useful, especially in experimental ultrasonic studies. The propagation and polarization vectors for modes propagated in pure directions, obtained by solution of the Christoffel equations[10] for antimony using the set of elastic constants measured here (Table I), are listed in Table II. For crystals belonging to the *RI* Laue group, both the $x$ and $z$ directions are pure-mode axes. The particle displacement vectors for the two pure $x$-axis shear modes can only be found from prior knowledge of the elastic moduli. The angle $\phi$ which the polarization vector makes with the $xy$ plane is given by

$$\tan\phi = U_3/U_1 = -C_{14}/(C_{44}-\rho v^2)\ . \tag{1}$$

Here $U_3$ and $U_1$ are the direction cosines of the polarization vectors obtained by substituting the measured velocities $v$ of the modes into this equation. The polarization vectors differ by $\pi/2$. In addition to the $z$ axis for one particular direction in the $yz$ plane, there is an accidental pure-mode axis whose direction, denoted $A$ in Table II, can be found from[10]

$$\frac{N_3}{N_2} = \frac{N_2^2C_{11}+N_3^2C_{44}-2N_2N_3C_{14}-\rho v_l^2}{N_2^2C_{14}-N_2N_3(C_{44}+C_{13})}\ , \tag{2}$$

where $v_l$ is the velocity of the longitudinal wave, and $N_3$ and $N_2$ are direction cosines of this propagation direction.

Explicit expressions for the hydrostatic and uniaxial pressure derivatives $-[\partial(\rho_0 W^2)/\partial p]_{P=0}$ at zero pressure in terms of the SOEC and TOEC for *RI* Laue-group rhombohedral crystals have been given by Thurston, McSkimin, and Andreatch.[15] The TOEC, computed for antimony using a least-mean-squares fit to the experimental data (Figs. 1 and 2), are compared with those of bismuth in Table III. The hydrostatic pressure derivatives of the SOEC are listed in Table IV.

## III. DISCUSSION

The *A*7 crystal structure may be regarded as being derived from the simple cubic structure by two consecutive distortions. (i) small extension along a body diagonal, reducing the rhombohedral angle $\alpha$ from 60°, and (ii) a

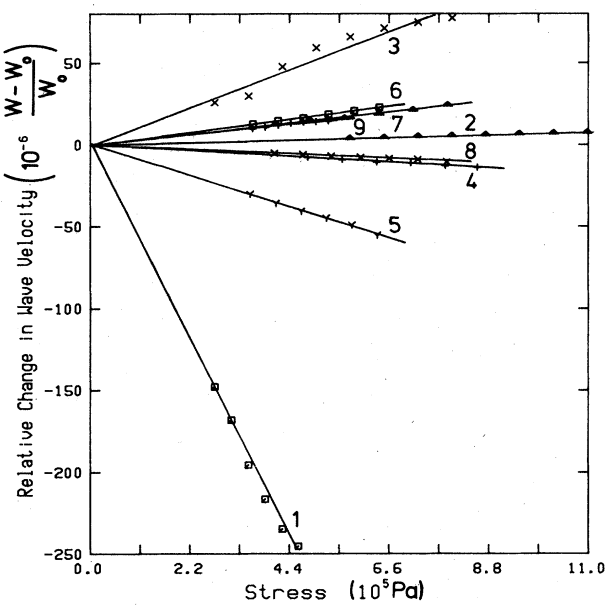


FIG. 2. Relative change in the natural wave velocity in antimony by the application of a uniaxial stress. The modes are (1) [001], [010], [100]; (2) [001], [100], [100]; (3) [001], [010], [010]; (4) [100], $[0\,-1/\sqrt{2}\,1/\sqrt{2}]$, $[0\,1/\sqrt{2}\,1/\sqrt{2}]$; (5) $[0\,1/\sqrt{2}\,1/\sqrt{2}]$, $[0\,-1/\sqrt{2}\,1/\sqrt{2}]$, [100]; (6) $[0\,1/\sqrt{2}\,1/\sqrt{2}]$, $[0\,-1/\sqrt{2}\,1/\sqrt{2}]$, $[0\,1/\sqrt{2}\,1/\sqrt{2}]$; (7) [100], $[0\,-1/\sqrt{2}\,1/\sqrt{2}]$, [100]; (8) $[0\,-1/\sqrt{2}\,1/\sqrt{2}]$, [100], [100]; (9) $[0\,1/\sqrt{2}\,1/\sqrt{2}]$, [100], [100], where in each case the first direction refers to that of the applied stress ($\vec{M}$), the second to that for wave propagation ($\vec{N}$), and the third to that for wave polarization ($\vec{U}$).

small movement of one face-centered rhombohedral sublattice along this body diagonal. The effects of these small distortions upon the physical properties of the group-V rhombohedral elements are considerable. Arsenic is the most distorted of the three semimetals ($\alpha = 54°10'$, $57°14'$, and $57°19'$ for arsenic, antimony, and bismuth, respectively). In fact, arsenic crystals have a surprising degree of layerlike character,[6] cleaving readily to expose (111) faces. In the $A7$ structure the planes occur in pairs in which atoms are comparatively close, the double layers being more widely separated. Although not strictly layerlike crystals, antimony and bismuth are markedly anisotropic. The thermal expansion, the elastic properties, the lattice dynamics, and the influence of pressure on lattice properties of the rhombohedral group-V elements can be more easily understood when this tendency towards layerlike behavior is kept in mind. For antimony the phonon dispersion curves determined from inelastic neutron scattering measurements[16] (including a substantial gap at the Brillouin-zone boundary between the acoustic and optic branches) are consistent with there being strong $p$-dominated bonds between each atom and its three nearest neighbors in a double-layer plane, while its bonds with the next nearest neighbors in the adjacent double layer are substantially weaker. The dynamics of phonon modes propagating in the trigonal direction are governed by the interplanar force constants because the double-layer planes move essentially as rigid bodies. The elastic stiffness constants of antimony (Table I) reflect the weaker interplanar forces in that $C_{11} > C_{33}$ and $S_{11} < S_{33}$. When hydrostatic pressure is applied, the $A7$ structure crystals progress towards the simple cubic structure;[17,18] then the layers tend to close up, changes in the interatomic spacings within the layers being much smaller. The linear compressibilities along the $z$ direction ($\beta_z$) and in the $z$ plane ($\beta_{xy}$) are markedly different:[6] for antimony $\beta_z$ $(=S_{33}+2S_{13})$ is $17.7\times10^{-12}$ $\mathrm{N^{-1}\,m^2}$ while $\beta_{xy}$ $(=S_{11}+S_{12}+S_{13})$ is much smaller at $3.6\times10^{-12}$ $\mathrm{N^{-1}\,m^2}$.

The higher-order elastic constants characterize the vibrational anharmonicity—the nonlinearity of interatomic forces with respect to displacements. In particular the adiabatic TOEC define the coefficients $[\partial^3 U(S,\eta)/\partial\eta_{ab}\partial\eta_{cd}\partial\eta_{ef}]_{S;\eta=0}$ of the cubic term in the expansion of the strain energy density $U(S,\eta)$ with respect to Lagrangian strain:

$$\rho_0 U(S,\eta) = \tfrac{1}{2} C^S_{abcd}\eta_{ab}\eta_{cd} + \tfrac{1}{6} C^S_{abcdef}\eta_{ab}\eta_{cd}\eta_{ef}\cdots . \quad (3)$$

At high temperatures especially, anharmonicity strongly influences physical properties, such as thermal expansion, which depend upon the thermal motion of the atoms. The marked anisotropy of the lattice properties of antimony extends to the TOEC: $C_{111} > C_{222} > C_{333}$ (Table III).

It is normal practice to discuss vibrational anharmonicity in terms of generalized Grüneisen parameters which measure the strain dependences of the lattice vibrational

TABLE I. Second-order adiabatic elastic stiffness constants and isothermal compliance constants of antimony at room temperature (293 K). Units of stiffness $10^9$ $\mathrm{N\,m^{-2}}$, compliance $10^{-12}$ $\mathrm{N^{-1}\,m^2}$.

| $C_{11}$ | $C_{12}$ | $C_{13}$ | $C_{14}$ | $C_{33}$ | $C_{44}$ | $C_{66}$ | Reference |
|---|---|---|---|---|---|---|---|
| 101.3±1.0 | 34.5±2.5 | 29.2±2.7 | 20.9±2.1 | 45.0±0.5 | 39.3±0.6 | 33.4±0.6 | This work |
| 99.4 | 30.9 | 26.4 | 21.6 | 44.5 | 39.5 | 34.2 | 12 |
| 79.2 | 24.7 | 26.1 | 11.0 | 42.7 | 28.5 | 27.3 | 13 |
| 81.0 | 11.0 | | 18.0 | 43.6 | 33.6 | 35.0 | 14 |
| $S_{11}$ | $S_{12}$ | $S_{13}$ | $S_{14}$ | $S_{33}$ | $S_{44}$ | $S_{66}$ | Reference |
| 16.3 | −6.1 | −6.6 | −11.9 | 30.9 | 38.1 | 44.7 | This work |
| 61.2 | −6.1 | −5.9 | −12.2 | 29.5 | 38.6 | 44.6 | 12 |
| 17.7 | −3.8 | −8.5 | −8.0 | 33.8 | 41 | 43 | 13 |

TABLE II. Character of acoustic modes propagated along the crystallographic and accidental pure-mode axes in antimony. $A$ denotes the accidental pure-mode direction in the $yz$ plane (orientation at 95° to the $z$ axis).

| Propagation direction | Mode type | Direction of polarization vector | Angular orientation of polarization vector | Mode velocity ($10^3$ m s$^{-1}$) | Mode Grüneisen parameter |
|---|---|---|---|---|---|
| $x$ | Pure shear (fast) | in $yz$ plane | 49° to $+y$<br>41° to $+z$ | 2.93 | −1.17 |
| $x$ | Pure shear (slow) | in $yz$ plane | 41° to $+y$<br>49° to $-z$ | 1.51 | −2.99 |
| $x$ | Pure longitudinal | $x$ | | 3.89 | −0.20 |
| $y$ | Pure shear | $x$ | | 2.23 | −1.67 |
| $y$ | Quasishear | in $yz$ plane | 73° to $+y$<br>17° to $+z$ | 2.22 | −1.46 |
| $y$ | Quasilongitudinal | in $yz$ plane | 17° to $+y$<br>73° to $-z$ | 4.01 | −0.27 |
| $z$ | Pure shear (degenerate) | in $xy$ plane | | 2.42 | −0.89 |
| $z$ | Pure longitudinal | $z$ | | 2.59 | +2.32 |
| $A$ | Pure shear | $x$ | | 2.11 | −1.83 |
| $A$ | Pure shear | in $yz$ plane | $A+\pi/2$ | 2.11 | −1.23 |
| $A$ | Pure longitudinal | in $yz$ plane | $A$ | 4.13 | −0.36 |

frequencies $\omega(p,\vec{q})$ accruing from the effect of hydrostatic pressure upon the lattice potential:

$$\gamma(p,\vec{q})=-\left[\frac{1}{\omega(p,\vec{q})}\left[\frac{\partial\omega(p,\vec{q})}{\partial\eta_{ij}}\right]_T\right]_{\eta=0}. \tag{4}$$

For acoustic modes at the long-wavelength limit, the vibrational anharmonicity can be described in the elastic continuum model.[19] In the case of a uniaxial crystal there are two independent components $\gamma_{11}$ $(=\gamma_{22})$ and $\gamma_{33}$ of the Grüneisen tensor. The scalar parameter $\gamma$ $(=\gamma_{11}+2\gamma_{33})$ is the weighted average of the individual mode gammas $\gamma(p,\vec{q})$:

$$\gamma=\sum_{p,\vec{q}}\gamma(p,\vec{q})c(p,\vec{q})\Big/\sum_{p,\vec{q}}c(p,\vec{q}), \tag{5}$$

where

$$c(p,\vec{q})=kx^2\exp(x)/[\exp(x)-1]^2,\quad [x=\hbar\omega(p,\vec{q})/kT]$$

is the contribution of a mode in branch $p$ and wave vector $\vec{q}$ to the specific heat of the crystal. In general the scalar $\gamma$ includes contributions from all the lattice modes including those on both the optic and acoustic branches at all wave vectors in the Brillouin zone. For a uniaxial crystal the Grüneisen parameter contributions from the acoustic modes alone can be obtained using[20]

$$\gamma^{\mathrm{Br}}=\sum_p\oint d\Omega\,\Gamma(p,\vec{N})C(p,\vec{N})\Big/\sum_p\oint d\Omega\,C(p,\vec{N}),$$
$$\gamma_\perp^{\mathrm{Br}}=\sum_p\oint d\Omega\,\Gamma_\perp(p,\vec{N})C(p,\vec{N})\Big/\sum_p\oint d\Omega\,C(p,\vec{N}), \tag{6}$$
$$\gamma_\parallel^{\mathrm{Br}}=\sum_p\oint d\Omega\,\Gamma_\parallel(p,\vec{N})C(p,\vec{N})\Big/\sum_p\oint d\Omega\,C(p,\vec{N}),$$

TABLE III. Third-order elastic constants of antimony in comparison with those of bismuth (Ref. 2). Units are $10^{11}$ N m$^{-2}$.

| | Antimony | Bismuth |
|---|---|---|
| $C_{111}$ | −21.1 ±0.5 | −7.14 |
| $C_{112}$ | 9.8 ±0.4 | 1.16 |
| $C_{113}$ | −1.87 ±0.3 | −1.78 |
| $C_{114}$ | 8.44 ±0.3 | −3.77 |
| $C_{123}$ | −4.18 ±0.9 | −1.27 |
| $C_{124}$ | −8.08 ±0.8 | −0.70 |
| $C_{133}$ | 3.81 ±0.4 | −1.62 |
| $C_{134}$ | −0.018±0.004 | 0.43 |
| $C_{144}$ | 2.94 ±0.5 | −0.50 |
| $C_{155}$ | −15.1 ±0.8 | −4.06 |
| $C_{222}$ | −11.5 ±0.6 | −5.77 |
| $C_{333}$ | −5.96 ±0.75 | −4.03 |
| $C_{344}$ | 2.72 ±0.56 | −0.95 |
| $C_{444}$ | 6.45 ±0.7 | 1.77 |

TABLE IV. Hydrostatic pressure derivatives of the second-order elastic stiffness tensor components of antimony at room temperature compared with those of bismuth (Ref. 2).

| | Antimony | Bismuth |
|---|---|---|
| $\partial C_{11}/\partial P$ | 10.8 ±0.2 | 6.38 |
| $\partial C_{12}/\partial P$ | 2.9 ±0.2 | 2.38 |
| $\partial C_{13}/\partial P$ | 6.7 ±0.4 | 4.69 |
| $\partial C_{14}/\partial P$ | 2.7 ±0.2 | 1.70 |
| $\partial C_{33}/\partial P$ | 8.0 ±0.2 | 6.62 |
| $\partial C_{44}/\partial P$ | 5.71±0.14 | 3.37 |
| $\partial C_{66}/\partial P$ | 3.90±0.14 | 2.00 |

where the superscript Br denotes the Grüneisen parameter introduced by Brugger, $||$ refers to the $z$ axis, and $\perp$ refers to the $z$ plane. In the high-temperature limit ($T > \Theta_D$) the heat capacity $C(p,\vec{N})$ per mode becomes equal to Boltzmann's constant $k$. This condition applies to antimony [$\Theta_D = 210$ K (Ref. 21)] at room temperature. For a rhombohedral crystal belonging to the $\bar{3}m$ ($RI$) Laue group, it can be shown that

$$\begin{aligned}\Gamma_{||}^{\mathrm{Br}}(p,\vec{N}) = -(B/2w)\{ & N_3 + 2w[(U_1^2+U_2^2)S_{13}+S_{33}U_3^2] + [S_{13}(C_{111}+C_{112})+S_{33}C_{113}](N_1U_1+N_2U_2)^2 \\ & + \tfrac{1}{2}[S_{13}(C_{222}-C_{112})+S_{33}(C_{113}-C_{123})](N_1U_2-N_2U_1)^2 + (2S_{13}C_{133}+S_{33}C_{333})N_3^2U_3^2 \\ & + [S_{13}(C_{144}+C_{155})+S_{33}C_{344}][(N_2U_3+N_3U_2)^2+(N_3U_1+N_1U_3)^2] \\ & + 2[S_{13}(C_{113}+C_{123})+S_{33}C_{133}](N_1N_3U_1U_3+N_2N_3U_2U_3) \\ & + 2[S_{13}(C_{114}+C_{124})+S_{33}C_{134}](N_1^2U_2U_3+2N_1N_2U_1U_3 \\ & + 2N_1N_3U_1U_2-N_2^2U_2U_3+N_2N_3U_1^2-N_2N_3U_2^2)\} , \end{aligned} \tag{7}$$

$$\begin{aligned}\Gamma_{\perp}^{\mathrm{Br}}(p,\vec{N}) = -(B/4w)\{ & N_1^2+N_2^2+2w[(S_{11}+S_{12})(U_1^2+U_2^2)+2S_{13}U_3^2] \\ & + [(S_{11}+S_{12})(C_{111}+C_{112})+2S_{13}C_{113}](N_1U_1+N_2U_2)^2 \\ & + [\tfrac{1}{2}(S_{11}+S_{12})(C_{222}-C_{112})+S_{13}(C_{113}-C_{123})](N_1U_2-N_2U_1)^2 \\ & + [2(S_{11}+S_{12})C_{133}+2S_{12}C_{333}]N_3^2U_3^2 \\ & + [(S_{11}+S_{12})(C_{144}+C_{155})+2S_{13}C_{344}][(N_2U_3+N_3U_2)^2+(N_3U_1+N_1U_3)^2] \\ & + 2[(S_{11}+S_{12})(C_{113}+C_{123})+2S_{13}C_{133}](N_1N_3U_1U_3+N_2N_3U_2U_3) \\ & + 2[(S_{11}+S_{12})(C_{114}+C_{124})+2S_{13}C_{134}](N_1^2U_2U_3+2N_1N_2U_1U_3 \\ & + 2N_1N_3U_1U_2-N_2^2U_2U_3+N_2N_3U_1^2-N_2N_3U_2^2)\} , \end{aligned} \tag{8}$$

where

$$\begin{aligned} w = {} & C_{11}(N_1U_1+N_2U_2)^2+C_{66}(N_1U_2-N_2U_1)^2+C_{33}N_3^2U_3^2 \\ & + C_{44}[(N_2U_3+N_3U_2)^2+(N_3U_1+N_1U_3)^2]+2C_{13}(N_1N_3U_1U_3+N_2N_3U_2U_3) \\ & + 2C_{14}(N_1^2U_2U_3+2N_1N_3U_1U_3+2N_1N_3U_1U_2-N_2^2U_2U_3+N_2N_3U_1^2-N_2N_3U_2^2) . \end{aligned}$$

Here $N_i$ and $U_i$ are direction cosines for the wave propagation and polarization directions; for any chosen propagation direction the polarization vector can be obtained as the eigenvector of the Christoffel equations; the eigenvalue corresponds to the mode velocity. The long-wavelength $\gamma^{\mathrm{Br}}(p,\vec{N})$ [$=\gamma_{||}^{\mathrm{Br}}(p,\vec{N})+2\gamma_{\perp}^{\mathrm{Br}}(p,\vec{N})$] for modes propagated in the $xz$, $yz$, and $xy$ planes of antimony, computed using Eqs. (7) and (8), are plotted in Fig. 3.

The high-temperature limit ($T > \Theta_D$) of the mean Grüneisen parameter can be obtained by a summation over all the zone-center modes $\gamma(p,\vec{q})$ on the acoustic phonon branch using

$$\gamma_H^{\mathrm{Br}} = \frac{1}{3N}\sum \gamma^{\mathrm{Br}}(p,\vec{q}) . \tag{9}$$

The summation has been carried out over 26 811 modes by dividing the Debye sphere into nearly equal areas with the mode propagation direction centered on each element. For antimony $\gamma_H^{\mathrm{Br}}$ is $-0.24$, the two components being $(\gamma_{\perp}^{\mathrm{Br}})_H = -0.56$ and $(\gamma_{||}^{\mathrm{Br}})_H = -0.08$.

A number of interesting features of the acoustic phonons of antimony are revealed by these Grüneisen parameters. In general, in the absence of mode softening the elastic constants and the lattice vibrational frequencies increase under hydrostatic pressure, which raises the strain free energy, so that normally the mode Grüneisen $\gamma$'s are positive. However, for antimony the mode Grüneisen $\gamma$'s are negative for propagation directions of elastic waves with wave vector $\vec{q}$ over large ranges of solid angles. The high anisotropy of $\gamma(p,\vec{q})$ and the tendency for many pure and quasishear modes to have negative $\gamma(p,\vec{q})$ can be accounted for in terms of the tendency for antimony to show layerlike characteristics. As the main effect of application of hydrostatic pressure is to squeeze the layers together ($\beta_z > \beta_{xy}$), the influence of the repulsive forces which act between the pairs of layers must be especially important. The work done against these forces requires that the energy and frequency of the longitudinal mode propagated down the $z$ axis should increase substantially when pressure is applied. Hence the mode Grüneisen parameter for this mode should be quite large and positive, while those for the $x$-axis longitudinal mode and $y$-axis

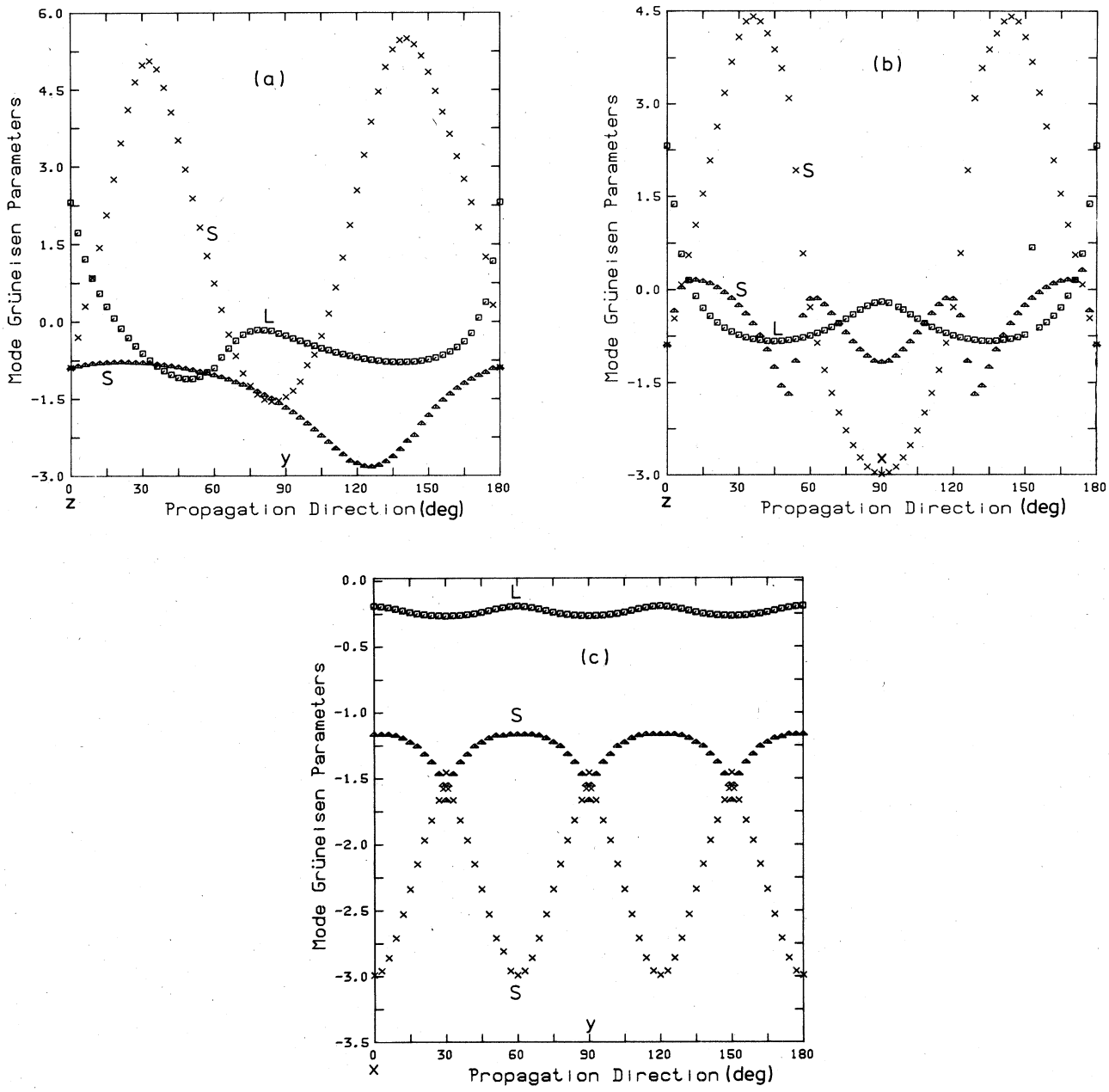


FIG. 3. Zone-center acoustic-mode Grüneisen parameter components as a function of mode propagation direction in the (a) *yz*, (b) *xz*, and (c) *xy* planes in antimony.

quasilongitudinal mode should be smaller—as they are (Table II). The relative contributions from SOEC and TOEC to the Grüneisen parameters for the longitudinal modes in the $z$ and $x$ directions can be seen by inserting the measured quantities into the particular expressions for these $\gamma_1$:

$$\gamma_L(z) = -(B/C_{33})[\,1+2C_{33}(S_{33}+2S_{13}) +2C_{133}(S_{11}+S_{12}+S_{13}) +(S_{33}+2S_{12})C_{333}\,], \quad (10)$$

$$\gamma_L(x) = -(B/2C_{11})[\,1+2C_{11}(S_{11}+S_{12}+S_{13}) +(C_{111}+C_{112})(S_{11}+S_{12}+S_{13}) +C_{113}(S_{33}+2S_{13})\,]. \quad (11)$$

Expressions similar to these have been given previously[2] but approximations made for bismuth have not been included here. Substitution of the measured SOEC (Table I) and TOEC (Table III) into the expression for $\gamma_L(z)$ shows that the terms including TOEC are substantially greater than those including SOEC only—the repulsive forces between the pairs of double layers do dominate the mode

Grüneisen parameter $\gamma_L(z)$ and hence the pressure dependence of this mode. The influence of the TOEC on $\gamma_L(x)$ is much less. The Grüneisen parameters of elastic modes propagated in directions in the $xy$ plane are particularly interesting in that all have anomalously negative values, those of modes which have longitudinal character being small but those of the shear-type modes being quite large. Qualitatively it can be seen that for those modes in which the double-layer planes of vibration act as almost rigid units in the $xy$ plane, the changing bond lengths tend to increase so that the corresponding Grüneisen parameters are negative. There is a marked shift towards more negative $\gamma(p,\vec{N})$, in antimony as compared with bismuth, especially for modes propagated in the $xy$ plane, a finding which conforms with the tendency of antimony to show more layerlike character.

This aspect of the lattice-dynamical behavior of antimony is reflected in the anisotropy of its thermal expansion. The component $\alpha_{33}$ along the $z$ direction is substantially larger than that ($\alpha_{11}=\alpha_{22}$) in the $xy$ plane because lower-energy lattice vibrations are more easily excited in the softer direction normal to the double-layer planes.[4,22,23] As the temperature is increased from a low value, the thermal expansion in the soft $z$ direction increases much more rapidly than in the hard directions in the $xy$ plane; in fact, $\alpha_{11}$ ($=\alpha_{22}$) is negative up to 20 K: Directions in the $xy$ plane actually contract as the temperature rises.[4] For a rhombohedral crystal of the *RI* Laue group, the principal thermal Grüneisen parameters are given by

$$\gamma^{\text{th}}=[(C_{11}+C_{12})\alpha_{11}+C_{13}\alpha_{33}]V/C_P\ , \tag{12}$$

$$\gamma^{\text{th}}=(2C_{13}\alpha_{11}+C_{33}\alpha_{33})V/C_P\ , \tag{13}$$

in directions in the $xy$ plane and along the $z$ axis, respectively. The temperature dependences of these parameters for antimony show that at low temperatures $\gamma_{\perp}^{\text{th}}(+0.5)<\gamma_{||}^{\text{th}}(+1.2)$ while at high temperatures $\gamma_{\perp}^{\text{th}}(+1.1)>\gamma_{||}^{\text{th}}(+0.9)$.[4] The crossover occurs at about 50 K. For uniaxial crystals at high temperatures, the Grüneisen parameter component tends to be larger along the directions associated with the stronger forces;[24] hence for antimony the weaker interlayer binding force results in $\gamma_{||}^{\text{th}}<\gamma_{\perp}^{\text{th}}$. Modes which depend chiefly upon strain in the weak-force direction tend to have smaller individual mode Grüneisen parameters $\gamma_i$ for this direction. However, the relative magnitudes of $\gamma_{\perp}^{\text{th}}$ and $\gamma_{||}^{\text{th}}$ cross over as the temperature is reduced because the highest-frequency modes (those in the directions of stronger bonding) are progressively frozen out. As the thermal expansion and the thermal Grüneisen parameter accrue from summation over all the lattice modes, relative contributions to each property from individual modes are difficult to assess. However, the acoustic-mode Grüneisen parameters (Fig. 3) provide the information necessary to determine the contributions from the zone-center acoustic phonons; at low temperatures the acoustic phonons dominate the phonon density and the thermal expansion. The elastic constants and acoustic-mode Grüneisen parameters should not be strongly dependent upon the temperature so that the room-temperature values of the latter should be reasonably similar to those at low temperatures. Bearing this in mind, the observation of a negative $\alpha_{11}$ at low temperatures can be directly associated with the fact that all the long-wavelength acoustic modes propagated in the $xy$ plane have negative Grüneisen parameters. Since these parameters are much larger for modes with shear than for those with longitudinal character, the results establish that the anomalous negative value of $\alpha_{11}$ below 20 K arises from the dominance of contributions from the zone-center transverse acoustic phonons at low temperatures.

Finally it is useful to comment upon the mode contributions to thermal expansion of antimony at room temperature. The high-temperature limits of the mean zone-center acoustic-mode Grüneisen parameter components [$(\gamma_{||}^{\text{Br}})_H=-0.56$ and $(\gamma_{\perp}^{\text{Br}})_H=-0.08$] are quite different from the thermal Grüneisen parameter components ($\gamma_{||}^{\text{th}}=+0.9$ and $\gamma_{\perp}^{\text{th}}=+1.1$). Since the Debye temperature [210 K (Ref. 21)] of antimony is quite low, at room temperature phonons will be excited throughout all states in the Brillouin zone in both optical and acoustic branches. The positive value of $\gamma^{\text{th}}$ ($=+0.97$) implies that the thermal expansion at room temperature involves substantial contributions from phonon states for which the mode Grüneisen parameters have the more usual positive sign, unlike many of those for the acoustic branches at long wavelength.


[1] W. Richter, T. Fjeldly, J. Renucci, and M. Cardona, in *Proceedings of the International Conference on Lattice Dynamics, Paris, 1977,* edited by M. Balkanski (Flammarion, Paris, 1978), p. 104.

[2] Tu Hailing and G. A. Saunders, Philos. Mag. **48**, 571 (1983).

[3] Tu Hailing and G. A. Saunders, J. Mater. Sci. **18**, 2337 (1983).

[4] G. K. White, J. Phys. C **5**, 2731 (1972).

[5] R. D. Brown, R. L. Hartman, and S. H. Koenig, Phys. Rev. **172**, 598 (1968).

[6] N. G. Pace, G. A. Saunders, and Z. Sümengen, J. Phys. Chem. Solids **31**, 1467 (1970).

[7] Y. K. Yoğurtçu, A. J. Miller, and G. A. Saunders, J. Phys. C **13**, 6585 (1980).

[8] R. N. Thurston and K. Brugger, Phys. Rev. **133**, A1604 (1964); **135**, AB3(E) (1964).

[9] Y. Eckstein, A. W. Lawson, and D. H. Reneker, J. Appl. Phys. **31**, 1534 (1960).

[10] N. G. Pace and G. A. Saunders, J. Phys. Chem. Solids **32**, 1585 (1971).

[11] A. J. Lichnowski and G. A. Saunders, J. Phys. C **10**, 3243 (1977).

[12] S. Epstein and A. de Bretteville, Phys. Rev. **138**, A771 (1965).

[13] P. W. Bridgman, Proc. Am. Acad. Arts Sci. **60**, 365 (1925).

[14] E. Leventhal, M. S. thesis, Polytechnic Institute of Brooklyn, 1959.

[15] R. N. Thurston, H.J. McSkimin, and P. Andreatch, J. Appl. Phys. **37**, 267 (1966).

[16] R. I. Sharp and E. Warming, J. Phys. F **1**, 570 (1971).

[17] B. Morosin and J. E. Schirber, Phys. Lett. **30A**, 512 (1969).

[18] B. Norin, Phys. Scr. **15**, 341 (1977).

[19]F. W. Sheard, Philos. Mag. **3**, 1381 (1958).
[20]K. Brugger and T. C. Fritz, Phys. Rev. **157**, 524 (1967).
[21]D. C. McCollum and W. A. Taylor, Phys. Rev. **156**, 782 (1967).
[22]H. D. Erfling, Ann. Phys. (Leipzig) **34**, 136 (1938).
[23]G. V. Bunton and S. Weintroub, J. Phys. C **2**, 116 (1969).
[24]R. W. Munn, Adv. Phys. **18**, 515 (1972).